Supplementary material for "Semiconductor-Metal Structural Phase Transformation in $MoTe_2$ Monolayers by Electronic Excitation"

Aravind Krishnamoorthy[1,*], Lindsay Bassman Oftelie[1,2], Rajiv K. Kalia[1,2,3,4], Aiichiro Nakano[1,2,3,4,5], Fuyuki Shimojo[6], Priya Vashishta[1,2,3,4]

[1]Collaboratory for Advanced Computing and Simulations, [2]Department of Physics, [3]Department of Computer Science [4]Department of Chemical Engineering and Material Science, [5]Department of Biological Sciences, University of Southern California, Los Angeles, CA 90089, [6]Department of Physics, Kumamoto University, Kumamoto 860-8555, Japan
**e-mail address: kris658@usc.edu*

Outline

1. Simulation methods
2. Dynamical stability of $MoTe_2$ monolayer under biaxial strain
3. Density of states of $MoTe_2$ H monolayer

Simulation methods

Optimization of crystal structures and calculation of ground state energies were done using density functional theory (DFT) with the projector augmented wave (PAW) [1] method implemented in the Vienna Ab initio Simulation Package (VASP) [2,3]. Activation energy barriers, defined as the energy difference between the H crystal structure and the configuration at the saddle point along the semiconducting-to-metal phase transition pathway, were calculated using the climbing image nudged elastic band method (CI-NEB) method implemented in the VASP Transition State Tools code [4].

Exchange and correlation effects are calculated using the Perdew–Burke–Ernzerhof form of the generalized gradient approximation to the exchange-correlation functional [5]. Valence electron wave functions are constructed using a plane wave basis set containing components up to a kinetic energy of 450 eV and the reciprocal space is sampled at the Γ point with a Gaussian smearing of orbital occupancies of 0.1 eV. All DFT calculations are conducted on a $6 \times 6 \times 1$ supercell of the $MoTe_2$ monolayer containing a total of 36 formula units (108 atoms) of $MoTe_2$. Monolayers are separated from their periodic images (in the out-of-plane direction) by a large vacuum of 20 Å to remove spurious image interactions. Calculations were performed till each self-consistency cycle is converged in energy to within 1×10^{-8} eV/atom and forces on ions are under 5×10^{-4} eV/Å.

Density of electronic states was plotted using DFT calculations on previously optimized $6 \times 6 \times 1$ $MoTe_2$ monolayer supercells where the reciprocal space was sampled using a dense Γ-centered $9 \times 9 \times 1$ k-point mesh and partial occupancies of eigenlevels are determined by the tetrahedron method [6]. Fermi surfaces of the H crystal in the ground and excited state are constructed from DFT calculations on a $1 \times 1 \times 1$ unitcell of the $MoTe_2$ monolayer performed at high-accuracy using a plane-wave cutoff of 650 eV and a Γ-centered $15 \times 15 \times 1$ k-point mesh.

Dynamical stability was inferred from the frequency of normal vibration modes of the H crystal structure. The Hessian matrix was generated within the formalism of density functional perturbation theory and dispersion relations for normal vibration modes were calculated using the open-source phonopy package [7]. For both NEB and phonon dispersion calculations, excited states are described within the Δ-SCF DFT framework. In this scheme, a non-Aufbau constraint is imposed on orbital occupancies to promote electrons from the occupied Kohn-Sham energy levels to unoccupied higher-energy levels followed by relaxation of nuclear positions to minima in the potential energy surface defined by the charge density corresponding to the fixed occupancy of these energy levels. The ΔSCF method is an inexpensive approximation to the potential energy surface of the excited state system with accuracy comparable to time-dependent density functional theory methods [8,9]. The ΔSCF method is widely used to describe spatially localized excited-state wavefunctions in isolated molecules, but can also characterize excitations in organic systems and semiconductor clusters and nanodots, where excited states are delocalized over several hundred atoms [10,11]. ΔSCF schemes have also been used to describe excited electronic states of adsorbates and crystal surfaces, where ground-state and excited wavefunctions are delocalized over the entire periodic supercell [12].

Dynamic stability under biaxial lattice strain

While elastic strain engineering can affect the relative stability of the H and T' polytypes, this change in the potential energy landscape was found to not significantly affect the dynamical stability of the ground state crystal. This is confirmed by a calculation of phonon dispersion relations of unstrained and strained H $MoTe_2$ films, which do not show any appreciable softening of vibration modes along important points along the hexagonal Brillouin zone. This high dynamical stability of the H polytype under strain implies the lack of low-energy atomic distortions that are necessary for the existence of a low-energy phase transition pathway.

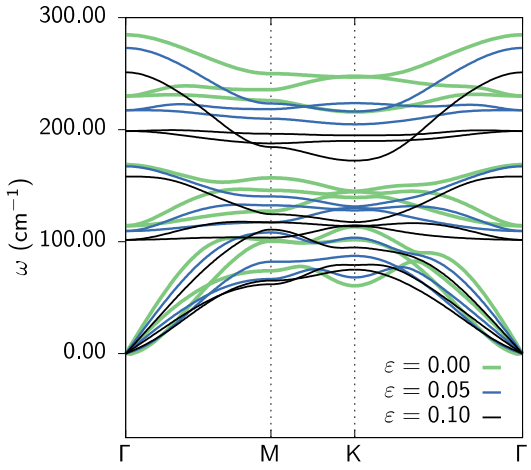

FIG. S1: A plot of the phonon band structure of monolayer $MoTe_2$ at three representative tensile lattice strains of $\varepsilon = 0.00, 0.05, 0.10$ shows no noticeable softening along high-symmetry paths in the first Brillouin zone.

Density of states of $MoTe_2$ H monolayer

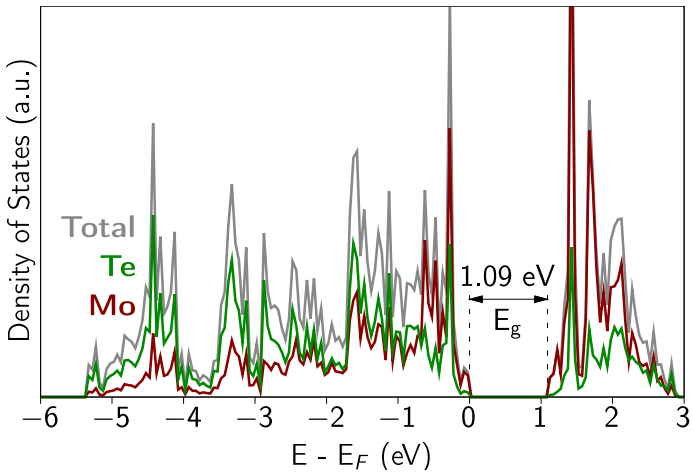

FIG. S2: Calculated density of electronic states in the $MoTe_2$ monolayer (gray). Red and blue lines show the density of states projected on to spheres of radius 2.15 Å centered on Mo and Te atoms respectively.

The calculated band gap of the $MoTe_2$ monolayer in our simulations is 1.09 eV, which is consistent with experimental values measured by optical means. The valence and conduction band edges are dominated by Mo d-states, which is consistent with observations from other monolayer TMC crystals.

Electronic structure of electron-doped $MoTe_2$ H monolayer

Figure S3 shows the phonon dispersion curve of electron-doped $MoTe_2$ H monolayer at three representative charge carrier concentrations of 0, 0.5 and 1.0 × 10^{14} cm^{-2}. n-type $MoTe_2$ monolayers show imaginary vibration frequencies at electron concentrations above 10^{14} cm^{-2}, identical to the case of electronically excited TMDCs. This similarity arises due to similarities in the Fermi surface and associated nesting vectors of the electronically-excited and electron-doped $MoTe_2$ monolayer.

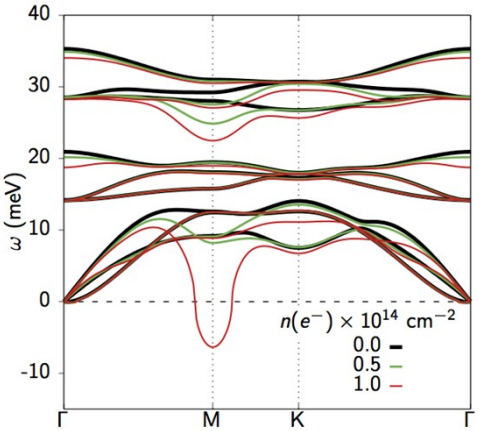

Figure S3: Phonon dispersion curve of electron-doped $MoTe_2$ monolayers at three different electron concentrations of n = 0, 0.5, 1.0 × 10^{14} cm^{-2} shows phonon softening at the M-point at high charge carrier concentrations, identical to electronically-excited monolayers.

To identify if photogenerated holes play a significant role in the strong electron-phonon coupling and phonon softening observed in electronically excited $MoTe_2$ monolayers, we plot the isosurface of hole states in the first Brillouin zone in Figure S4. These hole states are localized around the K-point in reciprocal space and do not show $\vec{\Gamma M}$ nesting vectors that could lead to softening of *M*-point phonons. This indicates that the observed phonon softening in electronically-excited and electron-doped $MoTe_2$ crystals results primarily from electron occupation of high-energy eigenlevels.

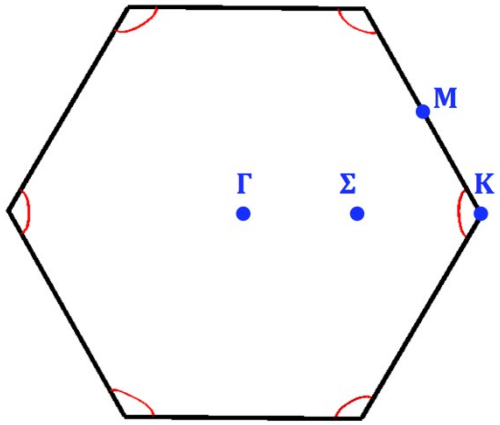

Figure S4: Isosurfaces of hole-states (red curves) in excited $MoTe_2$ monolayers are localized at the *K*-point and do not show nesting vectors along the $\vec{\Gamma M}$ direction, which are responsible for phonon softening at the *M*-point.

References

[1] P. E. Blöchl, Physical Review B **50**, 17953 (1994).

[2] G. Kresse and J. Furthmuller, Physical Review B **54**, 11169 (1996).

[3] G. Kresse and J. Furthmuller, Comp Mater Sci **6**, 15 (1996).

[4] G. Henkelman, B. P. Uberuaga, and H. Jonsson, Journal of Chemical Physics **113**, 9901 (2000).

[5] J. P. Perdew, K. Burke, and M. Ernzerhof, Physical Review Letters **77**, 3865 (1996).

[6] P. E. Blochl, O. Jepsen, and O. K. Andersen, Physical Review B **49**, 16223 (1994).

[7] A. Togo and I. Tanaka, Scripta Mater **108**, 1 (2015).

[8] T. Kowalczyk, S. R. Yost, and T. Van Voorhis, Journal of Chemical Physics **134**, 054128 (2011).

[9] J. Gavnholt, T. Olsen, M. Engelund, and J. Schiotz, Physical Review B **78**, 075441 (2008).

[10] T. Baruah, M. Olguin, and R. R. Zope, Journal of Chemical Physics **137**, 084316 (2012).

[11] M. Marsili, S. Botti, M. Palummo, E. Degoli, O. Pulci, H. C. Weissker, M. A. L. Marques, S. Ossicini, and R. Del Sole, Journal of Physical Chemistry C **117**, 14229 (2013).

[12] A. Hellman, B. Razaznejad, and B. I. Lundqvist, Journal of Chemical Physics **120**, 4593 (2004).